J Mater Sci (2008) 43:1966–1973
DOI 10.1007/s10853-008-2462-z

Combining MoS_2 or $MoSe_2$ nanoflakes with carbon by reacting $Mo(CO)_6$ with S or Se under their autogenic pressure at elevated temperature

Vilas G. Pol · Swati V. Pol · Pani P. George · Aharon Gedanken

Received: 23 November 2007 / Accepted: 8 January 2008 / Published online: 30 January 2008

Abstract This paper describes a non-aqueous, solvent-free, environmentally friendly, one-pot facile reaction to synthesize inorganic materials inclusion with carbon (MoS_2 or $MoSe_2$/C) at low temperatures. Nanoflakes of MoS_2 and $MoSe_2$ inclusion with carbon are prepared by a thermal (750 °C) reaction between $Mo(CO)_6$ and S or Se at their autogenic pressure in a closed reactor under inert atmosphere. Elemental sulfur or selenium powders are chosen in order to avoid the use of highly toxic H_2S and H_2Se gases. Without further processing of the as-prepared MoS_2/C or $MoSe_2$/C products, their compositional, morphological and structural characterization are carried out. The possibility of hydrogen storage in as-synthesized MoS_2/C or $MoSe_2$/C products is examined. A probable reaction mechanism for the formation of MoS_2 or $MoSe_2$ nanoflakes inclusion with C is discussed.

Introduction

Many scientists have devoted attention to the production of metaldichalcogenides [1–3] [MoX_2 (X = S, Se)], taking into account their unique physical and chemical properties. MoX_2 possesses a sandwich-like structure with X–Mo–X layers, which can also act as an intercalation host [4]. MoX_2 nanomaterials have application in heterogeneous catalysis [5], lubrication [6], and tribological applications [7]. The catalytic properties of nanostructured MoX_2 are size- and shape-dependent. The catalytic properties were studied for their onion-like, rod-like, or tubular morphologies [8, 9]. Nanocrystallites of $MoSe_2$ have been reported as effective compounds for the conversion of sunlight into electrical energy in photoelectrochemical cells [10].

A variety of techniques have been reported for the controlled synthesis of MoS_2, e.g., direct chemical synthesis [11], block copolymer micelles [12], electrosynthesis [13], laser ablation [14], microwave plasma [15], and solid-state reactions [16]. For $MoSe_2$, the reported synthetic procedures [17–19] are hydrothermal, electrosynthesis, inverse micelle, thermal decomposition, and laser ablation. All these techniques involve complicated process control and some of the techniques have produced amorphous MoX_2, which requires further heat treatment to induce crystallization. In recent years, carbon materials have found application as substrates to support various nanomaterials leading to functional carbon-based nanocomposites with specific electronic, magnetic, and optical properties [20]. This report on MoX_2/C nanocomposites may span a wide range of applications in various areas because they reap the benefits of corresponding MoS_2 or $MoSe_2$ with carbon materials.

The environmentally friendly, solventless, single-step, uncomplicated, and efficient reactions under autogenic pressure at elevated temperature (RAPET) approach is used for the fabrication of crystalline MoX_2 nanoflakes inclusion with carbon. The application of highly toxic H_2S and H_2Se gases is avoided by using S and Se powders and handling them under inert atmosphere inside a glove box. The mechanistic elucidation for the formation of anisotropic

V. G. Pol (✉) · S. V. Pol · P. P. George · A. Gedanken
Department of Chemistry and Kanbar Laboratory for Nanomaterials, Bar-Ilan University Center for Advanced Materials & Nanotechnology, Bar-Ilan University, Ramat-Gan, Israel
e-mail: vilaspol@gmail.com

MoS_2 or $MoSe_2$ particles inclusion with carbon is provided, based on the obtained analytical data, control experiments, and previously published reports. The possibility of hydrogen storage in RAPET-synthesized anisotropic MoS_2/C or $MoSe_2$/C products is tested.

Results and discussion

The XRD pattern of the MoS_2 nanoflake/C composite (MSNC) product is illustrated in Fig. 1a. The major peaks correspond to the reflection lines of the hexagonal phase of MoS_2 [space group = P63/mmc (194)]. These values match well with the literature powder diffraction file (PDF) 37-1492. Figure 1b shows the XRD diffraction pattern of the $MoSe_2$ nanoflake/C composite (MSeNC) sample. The reflection lines are in good agreement with the diffraction peaks, peak intensities, and the cell parameters of crystalline hexagonal $MoSe_2$ [space group = P63/mmc (194)] that match with the literature, PDF No. 29-914. Using the Debye–Scherrer equation to calculate the crystallite size, we found that the average nanocrystal size for an MSNC product is 8 nm and ca 16 nm for the MSeNC sample. Both XRD patterns reveal wide diffraction peaks, which are evidence of the formation of small nanoparticles of MoS_2 and $MoSe_2$. The absence of graphitic peaks indicates the possibility that carbon is present only as an amorphous phase.

The sulfur, carbon, and hydrogen content in the product/carbonaceous materials was determined by elemental analysis measurements. The calculated elemental (wt.) percentages of C, O, Mo, and S in the reaction mixture [$Mo(CO)_6$ and S] are 22.0, 29.5, 29, and 19.5%, respectively. In the as-prepared MSNC sample, the measured amount of carbon is 13.0 ± 2 wt.% and that of sulfur is 34 ± 2 wt.%. Additional evidence on composition is achieved by the bulk EDAX analysis of an MSNC sample (Fig. 1c). Since the X-ray energies for Mo (2.39 keV) and S (2.4 keV) are very close, we have obtained the overlapped single wide peak at 2.4 keV (Fig. 1c, left spectrum). The computer software attached to the EDAX measurements gave an S/Mo molar concentration ratio of ~2.

The calculated elemental (wt.) percentages of C, O, Mo, and Se in the reaction mixture [$Mo(CO)_6$ and Se] are 17.0, 22.7, 22.7, and 37.4%, respectively. We could determine the carbon and hydrogen content in the reaction product by elemental [C, H, N, and S] analysis and Mo, Se by EDAX. The measured amount of carbon in the as-prepared MSeNC sample is 5.2 wt.%. The measured oxygen amount is negligible in both the MSNC and MSeNC products. It is clear that the amount of carbon in the MSNC and MSeNC samples is reduced, as compared with the $Mo(CO)_6$ precursor, because CO_2 might have formed during the decomposition of the precursor that is liberated as a result of overpressure upon the opening of the Swagelok reactor. EDAX measurements gave a Se/Mo molar concentration ratio of 2 ± 0.1, which is in good agreement with the theoretical value of molybdenum diselenide stoichiometry (Fig. 1c, right spectrum).

SEM, SAEDX, elemental dot mapping (WDX) and surface area analysis

The morphologies of the MSNC and MSeNC products are primarily investigated by SEM measurements. The MSNC sample shows ~800 nm circular bodies with flakes/rods on the outer surfaces (Fig. 2a). The HR-SEM image (Fig. 2b) confirms that the flakes are 20 nm in thickness with a length of ~100 nm. These flakes are assembled in a typical morphology shows that the flakes are standing on the surfaces. To confirm the precise contents of the flakes, we used a wave-dispersive X-ray analyzer (WDX) that is much more sensitive to small elemental concentrations than the EDX technique that is attached to the SEM. The selected area SEM image for the elemental dot mapping (WDX) is shown in Fig. 2c. The contents of molybdenum, sulfur, and carbon are presented in Fig. 2d–f, respectively. These images verify the high percentage of Mo, S, and the lower percentage of carbon. It confirms that the formed flakes are composed of Mo, S, and C.

Figure 3a demonstrates the morphology of an MSeNC. It can be seen that the flakes are assembled to form a bulk particle of ~800 nm. The HR-SEM image of MSeNC (Fig. 3b) demonstrates that the nanoflakes have an average thickness of ~25 nm and the length is in the range of 150–200 nm. The area is selected for elemental dot mapping (WDX) from the SEM image as shown in Fig. 3c. The contents of the molybdenum, selenium, and carbon are presented in Fig. 3d–f, respectively. The higher percentage of Mo, Se, and the lower percentage of carbon is verified. This confirms that the formed assemblies are composed of Mo, Se, and C. The BET surface area for MSNC and MSeNC composites are 5 and 2.4 m^2/g, respectively.

TEM, HR-TEM, SAEDX, and electron diffraction analysis

The MSNC and MSeNC composites were further investigated by transmission electron micrograph (TEM) and HR-TEM measurements. The TEM of the MSNC composite shows the dark flakes overlying on other flakes with a faint contrast that are pointing out of the 400 nm diameter particle (Fig. 4a). A similar observation is noted for the MSeNC composite (Fig. 4b). The contradiction between

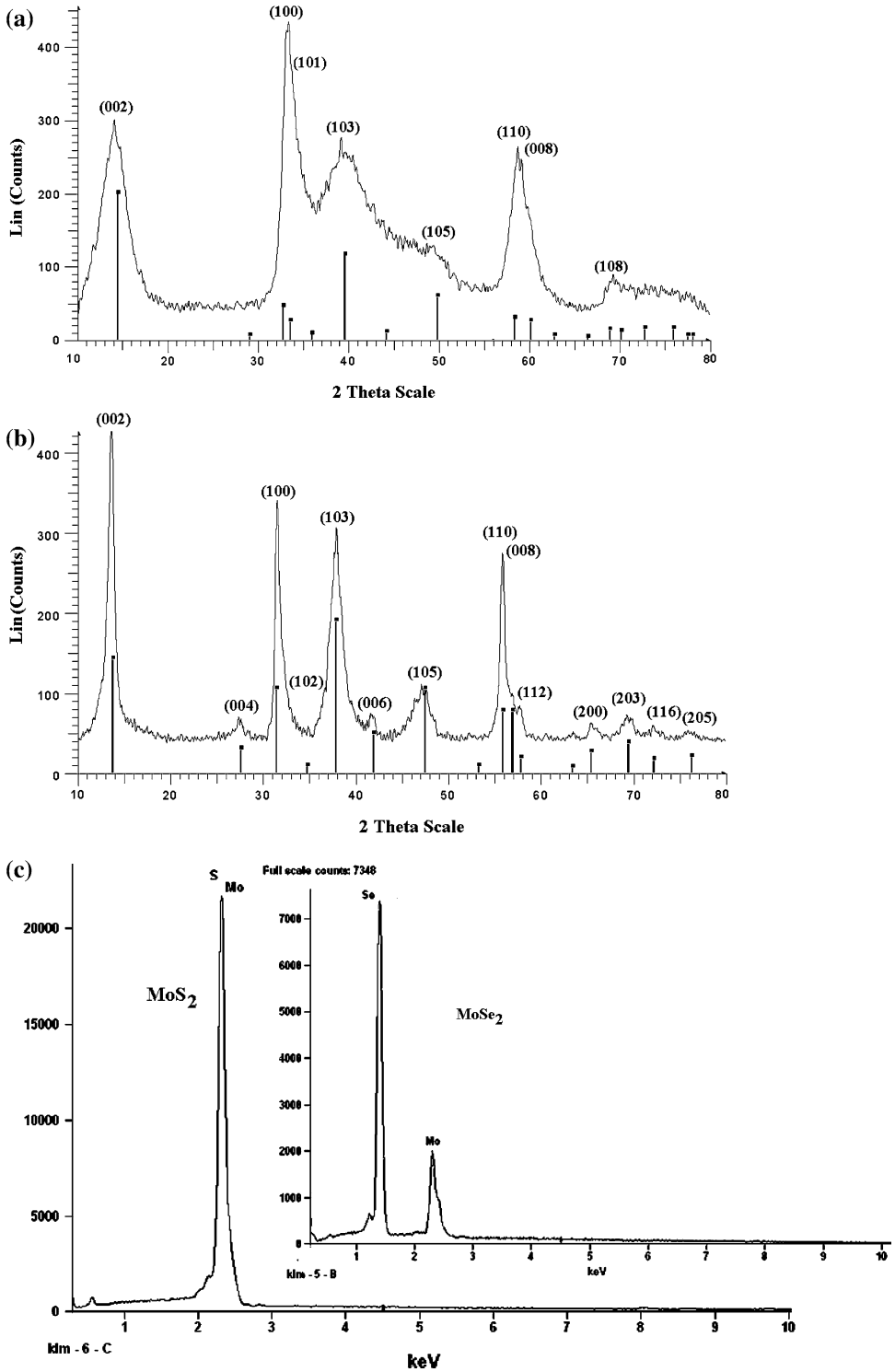

Fig. 1 XRD patterns of the thermally decomposed mixture of (**a**) [$Mo(CO)_6$ and S], (**b**) [$Mo(CO)_6$ and Se] at 750 °C under inert atmosphere, and (**c**) the EDAX spectra of MSNC (left) and MSeNC (right) composite

the XRD measurements and TEM crystal sizes observed in the TEM images can be explained as follows. The low-resolution TEM images although show bigger sizes of the particles, these particles are comprised of small flakes of chalcogenides, which clearly shown in the following HR-TEM images. The possibility of formation of amorphous chalcogenides is ruled out since 750 °C temperatures should suffice for the fabrication of crystalline MoS_2 or $MoSe_2$. Additionally, boiling points of S and Se are lower than the reaction temperature, therefore easy to react with highly reactive $W(CO)_6$ to form the respective chalcogenides in a closed reactor. Moreover, we should observe unreacted W in the XRD pattern if the S or Se is insufficient. Finally, we have taken stochiometric amounts of the

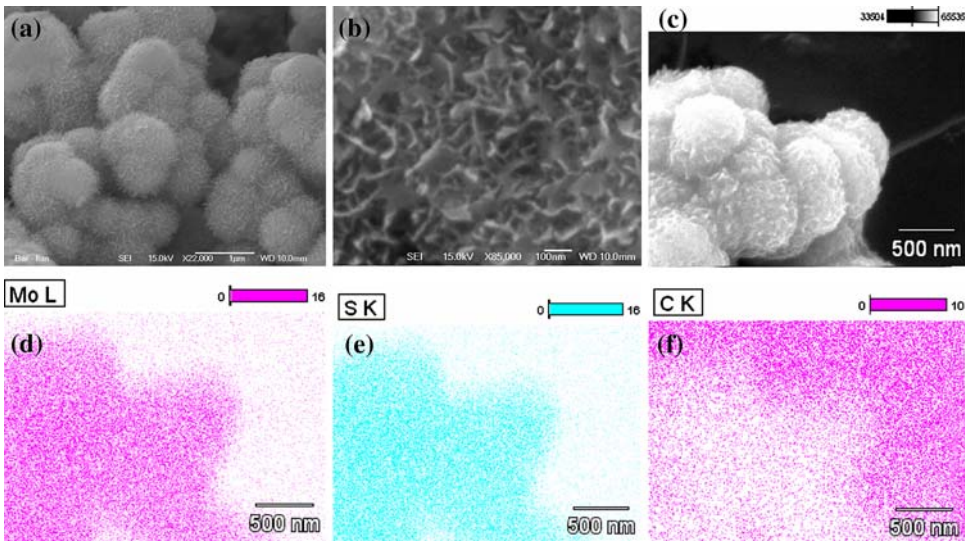

Fig. 2 SEM image of (**a**) MoS_2 nanoflakes/C composite (MSNC) (bar = 1 μm), (**b**) high-resolution image of an MSNC sample (bar = 100 nm), (**c**) selected image for X-ray dot mapping, (**d**) X-ray dot mapping for Mo, (**e**) X-ray dot mapping for S, (**f**) X-ray dot mapping for C on the selected image(**c**)

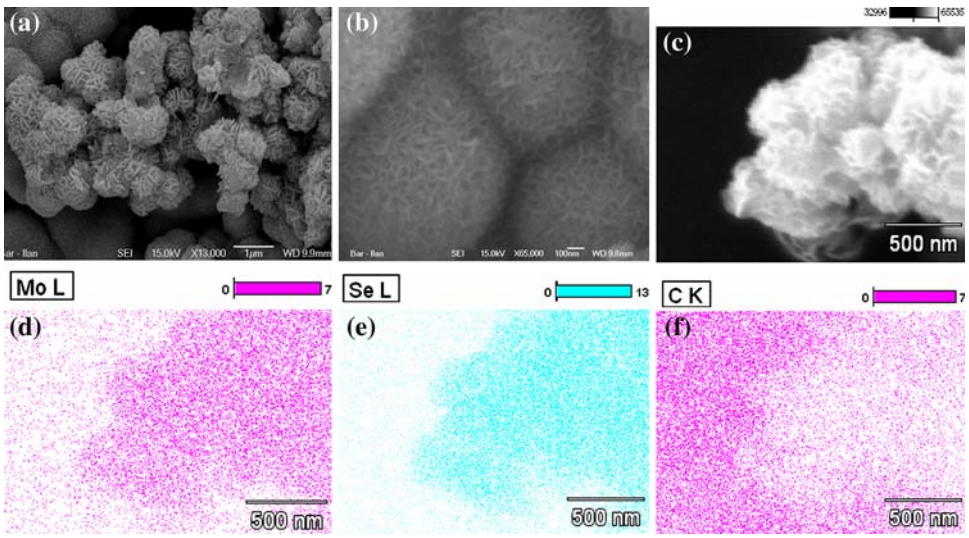

Fig. 3 SEM image of (**a**) an $MoSe_2$ nanoflake/C composite (MSeNC) (bar = 1 μm), (**b**) high-resolution image of MSeNC sample (bar = 100 nm), (**c**) selected image for X-ray dot mapping, (**d**) X-ray dot mapping for Mo, (**e**) X-ray dot mapping for Se, (**f**) X-ray dot mapping for C on the selected image (**c**)

reactants in a sealed reactor, no chance to liberate some materials that will lid to form non-stochiometric chalcogenides.

The as-formed MSeNC composite is comprised of 10–15 nanoflakes of average thickness in the range of 20–35 nm, with the lengths distributed between 100 and 200 nm. The faint carbon flakes are better seen in MSeNC than in MSNC. In order to identify the nanosized flakes inclusion with the carbon, we have measured the selected area EDS of an individual $MoSe_2$ nanoflake (Fig. 4c). The spectrum demonstrates the existence of 38.0 wt.% of Mo and 62.0 wt.% of Se, which is very close to the theoretical value of $MoSe_2$ (Mo = 37.8 wt.% and Se = 62.2 wt.%). The small carbon peak originates from the surrounding carbon matrix. We have also measured the selected area EDS outside the $MoSe_2$ nanoflakes (marked with an arrow in Fig. 4b). The spectrum (Fig. 4d) reveals a much higher percentage of carbon and a small percentage of Mo and Se. This result indicates that the $MoSe_2$ nanoflakes are surrounded by carbon. The Cu peaks originate from the carbon-coated Cu grid used as a sample support during TEM measurements.

Figure 4e demonstrates an HR-TEM image of a portion of a single $MoSe_2$ nanoflake. It illustrates the perfect arrangement of the atomic layers and the lack of defects. The measured distance between these (002) lattice planes is 0.634 nm, which is very close to the distance between the planes reported in the literature (0.646 nm) for the hexagonal lattice of the $MoSe_2$ [PDF No. 29–914]. The corresponding electron diffraction pattern is demonstrated in Fig. 4e. Figure 4f demonstrates that ~10 nm MoS_2 nanoflakes are inclusion with the carbon (marked by an arrow). Figure 4g shows the amorphous carbon at high resolution (marked by an arrow) surrounding the crystalline

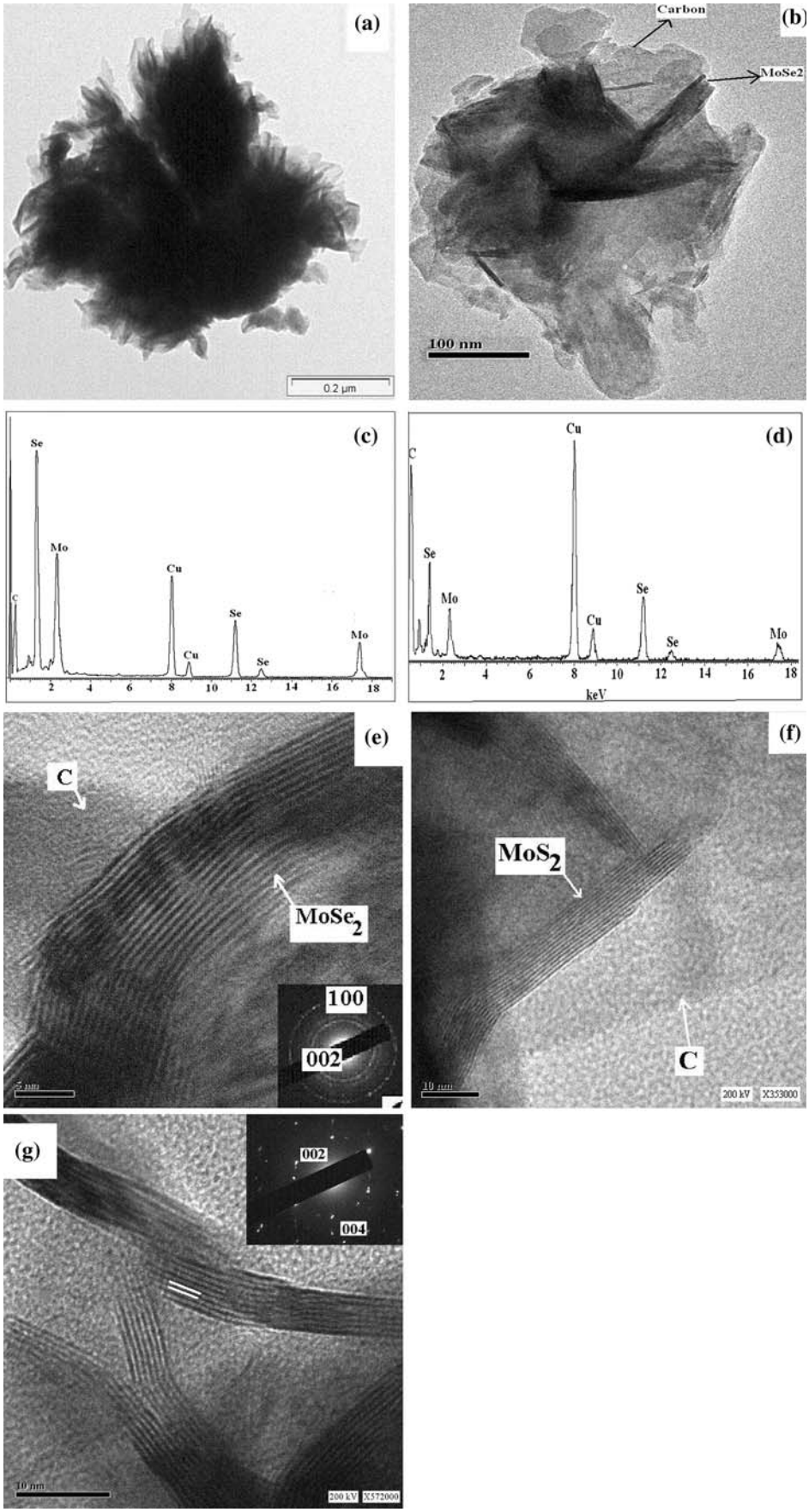

Fig. 4 TEM of (**a**) an MSNC composite, (**b**) an MSeNC composite, (**c**) SAEDS of $MoSe_2$, (**d**) SAEDS of surrounding carbon, (**e**) HR-TEM image of a single nanoflake of $MoSe_2$ (insert: SAED pattern), (**f**) HR-TEM image of MoS_2 nanoflake/C composite, and (**g**) MoS_2 nanoflakes inclusion with carbon (insert: SAED pattern)

MoS_2 fringes. The MoS_2 flakes assemble at around 8 nm, and the interlayer distance between the marked lines is 0.610 nm, very close to the literature value. An SAED pattern is inserted in Fig. 4g, and the detected planes of MoS_2 are assigned.

The explanation for the formation of MSNC and MSeNC products is based on the obtained analytical data, as well as on previously published data. From XRD, elemental (C, H, N, S) analysis, and SEM, HRSEM, TEM, and HR-TEM analysis, it is clear that the MSNC and MSeNC products are obtained as a result of the thermal dissociation [750 °C] of a mixture of $Mo(CO)_6$ and sulfur or selenium. We could not detect any morphological or structural changes in the products when the reaction time varied from 1 to 3 h. The reaction of $Mo(CO)_6$ without S or Se is known to result in the formation of Mo_2C and C [18]. Initially, the $Mo(CO)_6$ precursor undergoes thermal decomposition to afford Mo atoms and CO [$Mo(CO)_6 \rightarrow Mo + 6CO$]. According to the Boudouard reaction [21], the formed CO converts into the carbon and the CO_2 gas [$2CO \rightarrow C + CO_2$]. In addition, CO can react with Mo to form Mo_2C and C [$2Mo + CO \rightarrow Mo_2C + C$] [22].

In the current reaction, the formed Mo_2C will possibly react with the X (S and Se) according to $Mo_2C + 4X \rightarrow 2MoX_2 + C$. However, we suggest that perhaps in the presence of X (S and Se) carbide is not formed, because the reaction of metallic Mo with S and Se is so fast that it prevents the formation of the corresponding carbide. This is because MoS_2 and $MoSe_2$ are thermodynamically more stable than molybdenum carbide ($\Delta H^o_f = -53.0 \pm 3.97$, -55.7 ± 0.8, and -11.0 kcal/mole for MoS_2, $MoSe_2$, and Mo_2C, respectively) [23]. During the cooling of the Swagelok reactor, the formed MoS_2 or $MoSe_2$ is wrapped by the amorphous carbon. Under analogous reaction conditions, the thermal decomposition of $VO(OC_2H_5)_3$ and $MoO(OMe)_4$ produced V_2O_3 and MoO_2 cores, respectively, with a carbon shell. In both cases, the process is kinetically controlled, and V_2O_3 nanoparticles [24] or MoO_2 nanoparticles [25] show a higher solidification rate than carbon to form the core of the composite. Carbon, having a slower solidification rate, forms the shell layer. The carbon is amorphous since the temperature (750 °C) is not high enough to increase the crystallinity of the formed carbon. A similar reaction of $W(CO)_6$ with S under autogenic pressure at elevated temperature under inert atmosphere yielded worm-like WS_2 particles combined with carbon [26].

The hydrogen uptake by the anisotropic MoS_2/C and $MoSe_2$/C products prepared by the RAPET method is tested. The room temperature measurement is performed on a commercial pressure–composition (P–C) isotherm unit (Advanced Materials). Preliminary experiments (Fig. 5) revealed that $\sim$1.3 wt.% of H_2 can be adsorbed on the

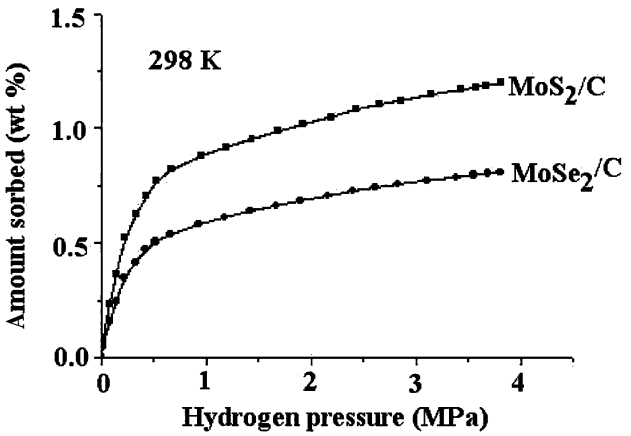

Fig. 5 Room temperature H_2 storage in MoS_2/C and $MoSe_2$/C products

MoS_2/C product, while 0.75 wt.% H_2 can be adsorbed in the $MoSe_2$/C product at room temperature and at 4 MPa. Recently, a 2.5 wt.% hydrogen storage capacity of RAPET-synthesized silicon carbide nanoflakes [27] (surface area 563 m^2/g) was reported at room temperature and at 6 MPa. Chen et al. [28] reported recently that multiwalled TiS_2 nanotubes with open-ended tips can absorb and desorb hydrogen reversibly with a capacity of 2.5 wt.% hydrogen. In our case, the low sorption of H_2 might be due to the low surface area of the materials.

In conclusion, avoiding the traditional use of highly toxic H_2S and H_2Se gases for the synthesis of MoS_2 or $MoSe_2$ is accomplished in the current study. The reactivity of elemental S and Se with $Mo(CO)_6$ at their autogenic pressure at 750 °C is demonstrated. This non-aqueous, solvent- and template-free reaction approach opens a facile route to synthesize inorganic nanoflakes inclusion with carbon (MoS_2 or $MoSe_2$/C) at relatively low temperatures, and which do not need further processing. A systematic compositional, morphological and structural characterization is carried out, and a plausible mechanism for the formation of MoS_2 or $MoSe_2$ nanoflakes with C is discussed. The maximum hydrogen sorption ($\sim$1.3 wt.%) is measured in a low-surface area MoS_2/C product.

Methods: synthesis of MoS_2 and $MoSe_2$ nanoflakes inclusion with carbon

The precursors, selenium, sulfur powder, and molybdenum hexacarbonyl [$Mo(CO)_6$], were purchased from Aldrich and used as received. For the synthesis of MoS_2 inclusion with C, a stoichiometric amount of 910 mg (3.4 mmole) of $Mo(CO)_6$ and 222 mg (6.8 mmol) of pure S powder is introduced into a 3 mL stainless steel reactor at room temperature in a nitrogen-filled glove box. For the synthesis of

$MoSe_2$ inclusion with C, a stoichiometric amount of 528 mg (2.0 mmol) of $Mo(CO)_6$ and 340 mg (4.3 mmol) of pure Se powder is introduced into a 3 mL stainless steel reactor, as above. The filled cells are tightly closed with the other plug (RAPET) [29, 30] and kept inside the 2.5″ diameter iron pipe inside the tube's furnace. The temperature of the tube's furnace is raised to 750 °C at a rate of 10 °C/min and maintained at 750 °C for 1–3 h. The Swagelok reactors heated at 750 °C are gradually cooled (~5 h) to room temperature, opened, and a black powder is obtained. About 662 mg of a black powder is obtained (58% yield) for MoS_2 with the C sample, termed as an MSNC. About 500 mg of a black powder is obtained (57% yield) for $MoSe_2$ with the C sample, termed as an [MSeNC]. Both crystalline products are directly characterized without further processing by various morphological, compositional, structural, and surface area analysis techniques.

Characterization

The X-ray diffraction patterns of the MSNC and MSeNC products are measured with a Bruker AXS D* Advance Powder X-ray diffractometer (using Cu $K\alpha = 1.5418$ Å radiation). The two methods used for the determination of the carbon and S content are C, H, N, S, and EDAX analysis. Elemental analysis of the samples was carried out on an Eager 200 °C, H, N, and S analyzer. The elemental composition of the materials and the SEM image were analyzed by an energy-dispersive X-ray analysis technique attached to JEOL-JSM 840 scanning electron microscope. The particle morphology and structure were studied by TEM on a JEOL-JEM 100 SX microscope, working at an 80 kV accelerating voltage, and with a JEOL-2010 HR-TEM instrument using an accelerating voltage of 200 kV. Samples for TEM and HR-TEM were prepared by ultrasonically dispersing the MSNC and MSeNC products separately into absolute ethanol, then placing a drop of this suspension onto a copper-grid coated with an amorphous carbon film, then drying under air. The surface area measurements were performed with a Micromeritics (Gemini 2375) surface area analyzer.

Acknowlegement A.G. thanks the Ministry of Science for financial support for this research via an Infrastructure Grant.

References

1. Tenne R, Margulis L, Genut M, Hodes G (1992) Polyhedral and cylindrical structures of tungsten disulfide. Nature 360:444
2. Amaratunga GAJ, Chhowalla M, Kiely CJ, Alexandrou I, Aharonow R, Devenish RM (1996) Hard elastic carbon thin films from linking of carbon nanoparticles. Nature 383:321
3. Nath M, Rao CNR (2002) Nanotubes of group 4 metal disulfides. Angew Chem Int Ed 41:3451
4. Nath M, Rao CNR (2001) New metal disulfide nanotubes. J Am Chem Soc 123:4841
5. Chianelli RR (1984) Fundamental-studies of transition-metal sulfide hydrodesulfurization catalysts. Catal Rev Sci Eng 26:361
6. Lince JR, Fleischauer PD (1999) A comparison of oxidation and oxygen substitution in MoS_2 solid film lubricants. Tribol Int 32:627
7. Tenne R (1995) Doped and heteroatom-containing fullerene-like structures and nanotubes. Adv Mater 7:965
8. Feldman Y, Wassermann E, Srolovitz DJ, Tenne R (1995) High-rate, gas-phase growth of MoS_2 nested inorganic fullerenes and nanotubes. Science 267:222
9. Feldman Y, Frey GL, Homyonfer M, Lyakhovitskaya V, Margulis L, Cohen H, Hodes G, Hutchison JL, Tenne R (1996) Bulk synthesis of inorganic fullerene-like MS_2 (M = Mo, W) from the respective trioxides and the reaction mechanism. J Am Chem Soc 118:5362
10. Homyonfer M, Mastai Y, Hershfinkel M, Volterra V, Hutchison JL, Tenne R (1996) Scanning tunneling microscope induced crystallization of fullerene-like MoS_2. J Am Chem Soc 118:7804
11. Duphil D, Bastide S, Levy-clement C (2002) Chemical synthesis of molybdenum disulfide nanoparticles in an organic solution. J Mat Chem 12:2430
12. Loginova TP, Kabachii YA, Sidorov SN, Zhirov DN, Valetsky PM, Ezernitskaya MG, Dybrovina LV, Bragina TP, Lependina OL, Stein B, Bronstein LM (2004) Molybdenum sulfide nanoparticles in block copolymer micelles: synthesis and tribological properties. Chem Mater 16:2369
13. Sen R, Govindaraj A, Suenaga K, Suzuki S, Kataura H, Iijima S, Achiba Y (2001) Encapsulated and hollow closed-cage structures of WS_2 and MoS_2 prepared by laser ablation at 450–1050 °C. Chem Phys Lett 340:242
14. Margulis L, Salitra G, Tenne R, Talianker M (1993) Nested fullerene-like structures. Nature 365:113
15. Vollath D, Szabo DV (1998) Synthesis of nanocrystalline MoS_2 and WS_2 in a microwave plasma. Mater Lett 35:236
16. Wiley JB, Kaner RB (1992) Rapid solid-state precursor synthesis of materials. Science 255:1093
17. Zhan JH, Zhang ZD, Qian XF, Wang C, Xie Y, Qian YT (1999) Synthesis of $MoSe_2$ nanocrystallites by a solvothermal conversion from MoO_3. Mater Res Bull 34:497
18. Huang DF, Kelley DF (2000) Synthesis and characterization of $MoSe_2$ and WSe_2 nanoclusters. Chem Mater 12:2825
19. Nath M, Rao CNR (2001) $MoSe_2$ and WSe_2 nanotubes and related structures. Chem Commun 2236–2237
20. Hu J, Li H, Huang X (2005) Influence of micropore structure on Li-storage capacity in hard carbon spherules. Solid State Ionics 176:1151
21. Laosiripojana N, Assabumrungrat S (2005) Applied, methane steam reforming over Ni/Ce-ZrO2 catalyst: influences of Ce-ZrO2 support on reactivity, resistance toward carbon formation, and intrinsic reaction kinetics. Catal A Gen 290:200
22. Moitei M, Calderon-Moreno J, Gedanken A (2002) Forming multiwalled carbon nanotubes by the thermal decomposition of $Mo(CO)_6$. Chem Phys Lett 357:267
23. Bailer JC, Emeleus HJ, Nyholm SR (1973) In: Trotman-Dickensor AF (ed) Comprehensive inorganic chemistry, 3rd edn. Pergamon Press, New York
24. Pol SV, Pol VG, Gedanken A (2004) Reactions under autogenic pressure at elevated temperature produces core shell structures of metals/metal oxides with carbon from various alkoxides. Chem Eur J 10:4467
25. Pol SV, Pol VG, Kessler VG, Seisenbaeva GA, Sung MG, Asai S, Gedanken A (2004) The effect of a magnetic field on a RAPET (Reaction under Autogenic Pressure at Elevated Temperature) of $MoO(OMe)_4$: fabrication of MoO_2 nanoparticles coated with

carbon or separated MoO_2 and carbon particles. J Phys Chem B 108:6322
26. Pol VG, Pol SV, Perkas N, Gedanken A (2007) WS_2 breeds with carbon to create worm-like nanostructure and assembly: reaction of W(CO)6 with S under autogenic pressure at elevated temperature in an inert atmosphere. J Phys Chem C 111:134
27. Pol VG, Pol SV, Gedanken A, Lim SH, Zhong Z, Lin JJ (2006) Thermal decomposition of commercial silicone oil to produce high yield high surface area SiC nanorods. Phys Chem B 110:11237
28. Chen J, Suo-Long Li, Zhan-Liang Tao, Yu-Tian Shen, Chun-Xiang Cui (2003) Titanium disulfide nanotubes as hydrogen-storage materials. J Am Chem Soc 125:5284
29. Pol SV, Pol VG, Gedanken A (2006) Testing of carbon-coated VO_x prepared via RAPET as Li insertion materials. Adv Mater 18:2023
30. Pol SV, Pol VG, Gedanken A (2006) Synthesis of WC nanotubes. Adv Mater 18:2023